Available online at www.sciencedirect.com
SCIENCE DIRECT
International Journal of Heat and Mass Transfer 49 (2006) 2912–2923
International Journal of HEAT and MASS TRANSFER
www.elsevier.com/locate/ijhmt

Laminar flow and heat transfer in a periodic serpentine channel with semi-circular cross-section

Nathan R. Rosaguti, David F. Fletcher *, Brian S. Haynes

Department of Chemical Engineering, University of Sydney, Sydney NSW 2006, Australia

Received 21 June 2005; received in revised form 10 February 2006
Available online 17 April 2006

Abstract

Computational fluid dynamics (CFD) has been used to study fully developed laminar flow and heat transfer behaviour in periodic serpentine channels with a semi-circular cross-section. The serpentine elements are characterised by their wavelength ($2L$), channel diameter (d) and radius of curvature of bends (R_c), with results reported for Reynolds numbers (Re) up to 450, as well as for a range of geometric configurations ($3 < L/d < 12.5$, $0.525 < R_c/d < 2.25$) at $Re = 110$. The flow in these channels is characterised by the formation of Dean vortices following each bend. As the Reynolds number is increased, more complex vortical flow patterns emerge and the flow domain becomes increasingly dominated by these vortices. Alignment of flow with vorticity leads to efficient fluid mixing and high rates of heat transfer.

Constant wall heat flux (H2) and constant wall temperature (T) boundary conditions and a range of fluid Prandtl numbers ($0.7 < Pr < 100$) have been examined. High rates of heat transfer and low pressure loss are found relative to fully-developed flow in a straight pipe, with heat transfer enhancements greater than 10 for a Prandtl number of 100.

As part of this work, we also obtain an accurate value for the Nusselt number for fully-developed flows in straight semi-circular passages with constant wall temperature, $Nu_T = 3.323(\pm 0.001)$.

Keywords: Serpentine; Heat transfer; CFD; Fluid flow; Enhancement

1. Introduction

It is well known that flows in curved passages, such as those which occur in coiled pipes, give rise to heat transfer enhancement relative to flow in straight pipes. While higher frictional losses are inevitably incurred in producing such flows, Kalb and Seader [1] and Masliyah and Nandakumar [2] have shown that the heat transfer enhancements can exceed the relative pressure-drop penalty by a significant amount (by factors of 2 or more for water) for laminar flows with constant axial heat flux and peripherally uniform temperature. The establishment of secondary flows (Dean vortices) in curved passages, underpinning this "low cost" improved laminar heat transfer performance, is attracting increasing interest in microchannel flow systems as a means not only of enhancing heat transfer but also of promoting mixing [3].

We recently characterised the thermo-hydraulic performance of serpentine passages with a circular channel cross-section [4] and showed that the establishment of Dean vortices at the bends in this geometry give rise to significant heat transfer enhancement which, in the absence of the creation of recirculation zones, can be achieved with a very small relative pressure-drop penalty. For the H2 boundary condition of Shah and London [5] (corresponding to uniform wall heat flux throughout, but in the absence of peripheral wall conduction), the Nusselt number for the flow of water with $Re = 110$ could be approximately twice that in the corresponding straight passage with only about 40% increase in frictional pressure drop.

* Corresponding author. Tel.: +61 2 93514147; fax: +61 2 93512854.
E-mail address: d.fletcher@usyd.edu.au (D.F. Fletcher).

0017-9310/$ - see front matter © 2006 Elsevier Ltd. All rights reserved.
doi:10.1016/j.ijheatmasstransfer.2006.02.015

Nomenclature

c_p	heat capacity [J kg^{-1} K^{-1}]
d	passage diameter [m]
d_h	hydraulic mean diameter [m]
Dn	Dean number $= Re(d/R_c)^{1/2}$ [–]
e_f	relative pressure-drop penalty [–]
e_{Nu}	relative heat transfer enhancement [–]
f	Fanning friction factor [–]
h	local heat transfer coefficient [W m^{-2} K^{-1}]
$\bar{h}_s$	axially local, peripherally-averaged heat transfer coefficient [W m^{-2} K^{-1}]
$\bar{h}_M$	mean heat transfer coefficient [W m^{-2} K^{-1}]
H_n	normalised helicity [–]
$\overline{H}_V$	volume-average of the absolute value of normalised helicity [–]
k	thermal conductivity [W m^{-1} K^{-1}]
L	serpentine half wavelength [m]
$\dot{m}$	mass flow rate [kg s^{-1}]
Nu	Nusselt number $= hd_h/k$ [–]
$\bar{p}$	area-averaged pressure [Pa]
P	cross-section perimeter [m]
q''	wall heat flux [W m^{-2}]
Pr	Prandtl number $= c_p\mu/k$ [–]
R_c	radius of curvature [m]
Re	Reynolds number $= \bar{u}_s\rho d_h/\mu$ [–]
s	axial location along the channel [m]
S	length of the channel [m]
$T_{x,y}$	temperature at a point (x,y) in a cross-section of the duct [K]
T_W	wall temperature [K]
$\overline{T}_B$	bulk mean temperature [K]
ΔT_S	temperature rise along one period of the channel [K]
u_s	velocity in the direction of s [m s^{-1}]
$\mathbf{v}$	velocity [m s^{-1}]
V	volume of serpentine channel unit [m^3]

Greek symbols

θ	non-dimensional temperature [–]
μ	dynamic viscosity [Pa s]
ρ	fluid density [kg m^{-3}]
$\boldsymbol{\omega}$	vorticity [s^{-1}]

Subscripts

B	bulk
M	mean
th	thermal
W	wall
x,y	(x,y) location on a cross-section

The circular section, whilst relevant to pipe networks, does not represent particularly well the channel cross-sections being produced in microchannel devices. These devices are often based on plate structures in which passages have been produced via chemical or mechanical means. Once the plates are stacked, the channels have a flat face and sharp corners, which, for etched passages, is well represented by a semi-circle. The impact of these characteristics on the relative heat transfer and pressure drop performance of such channels has not been quantified previously.

The geometry under consideration is illustrated in Fig. 1. The channel is defined by sweeping a semi-circle along a serpentine path with the flat face of the semi-circle being in the swept plane, and is fully characterised by the serpentine wavelength ($2L$), channel diameter (d) and the radius of curvature (R_c) of the bends. Dimensional similitude is achieved with constant ratios L/d and R_c/d. The hydraulic diameter, on which both the Reynolds and Nusselt numbers are based, is given by

$$d_h = \frac{\pi}{\pi+2}d \tag{1}$$

Repetitive or periodic geometric modules (Fig. 1) in compact heat exchangers lead to fully-developed flow after a sufficient number of modules, beyond which flow patterns become invariant at successive downstream locations. We consider such fully-developed flows, subject also to the constraint that the non-dimensional temperature profiles are invariant from one module to the next.

There have been a number of studies of laminar flow and heat transfer in straight ducts with circular-segment and circular-sector cross-sections [5–13] which include the semi-circular duct section as a particular case. The Fanning friction factor for fully-developed flow in the semi-circular case is given by $fRe = 15.772$ [6], which is very close to the

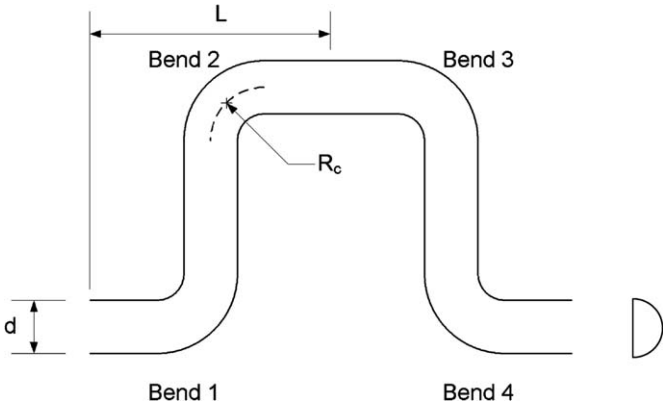

Fig. 1. Schematic of a repeating module of the serpentine geometry showing its axial and cross-sectional shape. The non-dimensional geometrical parameters of interest are L/d and R_c/d.

early work of Sparrow and Haji-Sheikh [7] that is cited in the compilation of Shah and London [5].

The Nusselt number for fully-developed flow within ducts of semi-circular cross-section for the case of constant wall heat flux appears also to be well established. In the presence of strong peripheral conduction (the "H1" condition [5]), $Nu_{H1} = 4.089$ [6] while in the absence of peripheral conduction ("H2" boundary condition [5]), $Nu_{H2} = 2.923$ [6]. The Nusselt number for uniform wall temperature (the "T" boundary condition [5]) is not well established, with reported values lying in the range of 3.316–3.684 [6].

In this paper, we report the effect of Reynolds and Prandtl numbers, as well as geometric configuration, on fully-developed flow and heat transfer in a serpentine channel with a semi-circular cross-section for the H2 and T boundary conditions.

2. Solution methodology

Numerical analyses of fully-developed laminar flow and heat transfer in geometries that are periodically repetitive in the streamwise coordinate have been carried out using the finite-volume CFD code ANSYS CFX-5.7® [8]. This code solves the Navier Stokes and energy equations on an unstructured mesh using a vertex based finite volume method together with a modified Rhie–Chow algorithm to link the pressure and velocity fields, which are solved via a coupled solver. The resulting algebraic equations are solved via an Algebraic Multigrid method. All calculations are performed using a second-order bounded differencing scheme for the convective terms.

In order to simulate fully-developed conditions, we wrap the velocities (u, v, w) and scaled temperatures from the outlet of the serpentine unit to the inlet. As gradient information is not wrapped, the flow is never properly developed. We allow for sufficient entrance length by modelling three serpentine modules (Fig. 1) such that fully developed flow is achieved in the centre module. Results reported here are extracted from the converged solution for the middle domain [4]. Temperature fields are scaled to allow calculation of the fully developed temperature field by imposing the condition that the non-dimensional temperature is equal at both the inlet and the outlet of the repeating unit of interest:

$$\theta_{in} = \left(\frac{\overline{T}_W - T_{x,y}}{\overline{T}_W - \overline{T}_B}\right)_{in} = \left(\frac{\overline{T}_W - T_{x,y}}{\overline{T}_W - \overline{T}_B}\right)_{out} = \theta_{out} \tag{2}$$

where

$$\overline{T}_W = \frac{1}{P}\int_p T_W \, dp \tag{3}$$

is the perimeter-averaged wall temperature at an axial location s, and

$$\overline{T}_B = \frac{1}{\dot{m}c_p}\int_{A_s} \rho u_s c_p T_{x,y} \, dA_s \tag{4}$$

is the bulk mean temperature at an axial location s, with $T_{x,y}$ being the temperature at location (x, y) in the section at s.

2.1. T boundary condition

For the case of *constant wall temperature*, T_W is constant, and the following form of Eq. (2) is used to determine the required inlet temperatures:

$$T_{x,y}|_{in} = T_W - (T_W - \overline{T}_B|_{in})\left(\frac{T_W - T_{x,y}|_{out}}{T_W - \overline{T}_B|_{out}}\right) \tag{5}$$

where T_W and $\overline{T}_B|_{in}$ are specified and $\overline{T}_B|_{out}$ is obtained from the simulation.

2.2. H2 boundary condition

For the case of *constant wall heat flux*, temperature profiles are identical in shape at the entrance and exit, but are displaced by an amount that is proportional to the wall heat flux and the wall area. The mean wall temperature, $\overline{T}_W$, in this case, varies along the axial path s. As temperature profiles are identical in shape

$$T_{x,y}|_{out} - T_{x,y}|_{in} = \Delta T_S \tag{6}$$

An overall heat balance gives

$$\overline{T}_B|_{out} - \overline{T}_B|_{in} = \frac{q'' A}{\dot{m}c_p} \tag{7}$$

So

$$\Delta T_S = \frac{q'' A}{\dot{m}c_p} \tag{8}$$

The desired inlet temperatures are determined from scaled outlet temperatures through the use of Eqs. (5) and (6) for fully-developed flow in the modules.

2.3. Model discretisation

In discretising the model domain, a swept hexahedral mesh has been used for the purposes of computational efficiency and accuracy. The cross-sectional mesh was constructed heuristically to provide greatest resolution in areas containing the greatest velocity and temperature gradients. As expected, the mesh is most refined in the vicinity of the walls, as shown in Fig. 2(a). The mesh on the inlet face was extruded along the axial path s to produce the swept mesh shown in Fig. 2(b). The axial mesh was also distributed to provide accurate resolution of the flow throughout the domain.

The grid independence of the computational results was tested by comparing velocity and temperature profiles at specific points within the geometry. Typical results of this study can be seen in Fig. 3, showing non-dimensional temperature profiles one diameter (1d) downstream of Bend 1 for $Re = 200$, $Pr = 6.13$ along the radius normal to the baseline chord of the semi-circle. The mesh used in this

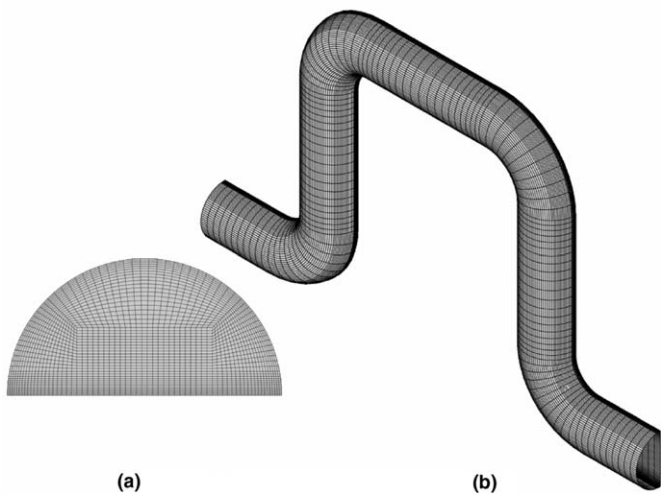

Fig. 2. Mesh density (a) on a cross-section and (b) along the axial direction.

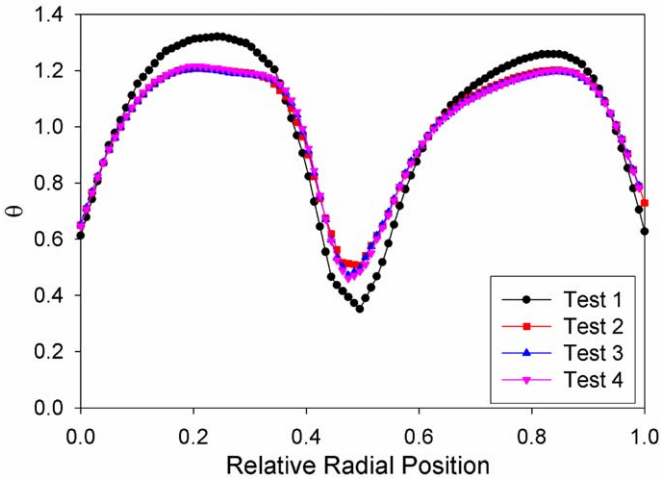

Fig. 3. Non-dimensional temperature profiles perpendicular to the flow axis 1d downstream of Bend 1 for increasing mesh density. $Re = 200$, $Pr = 6.13$. The number of volume elements for Tests 1–4 is: 108,000, 177,000, 245,000, and 291,000, respectively.

study contains approximately 2100 elements on the inlet cross-section, as shown in Fig. 2(a), with the repeating unit having more than 245,000 volume elements, Fig. 2(b). Tests were carried out at higher Reynolds and Prandtl numbers, as gradients of both velocity and temperature increase with these parameters. Tests indicate that for $Re = 450$ and $Pr = 100$, further increases in grid refinement by 12% (of volume elements) resulted in a change in the mean heat transfer coefficient of the serpentine unit by less than 1.5%. This decreases with Reynolds number, with no effect at lower Prandtl numbers.

3. Results

A number of heat transfer coefficients are defined in order to evaluate the heat transfer performance of the serpentine channel. Local (h), peripherally-averaged axially local ($\bar{h}_s$), and mean ($\bar{h}_M$) values are calculated. The local heat transfer coefficient is defined as

$$h = \frac{q''_w}{T_w - \overline{T}_B} \tag{9}$$

The peripherally-averaged heat transfer coefficient at a given axial location s is defined as

$$\bar{h}_s = \frac{\bar{q}''_w}{\overline{T}_w - \overline{T}_B} \tag{10}$$

Mean heat transfer coefficients for the repeating unit of interest can then be calculated from the axially-weighted average values of $\bar{h}_s$ by

$$\bar{h}_M = \frac{1}{S}\int_s \bar{h}_s \, ds \tag{11}$$

We assess the performance of the serpentine channel by comparing pressure drop and rate of heat transfer in these passages to the same quantities arising in fully-developed flow in a straight pipe of equal path length and diameter. We define the heat transfer enhancement as

$$e_{Nu} = \frac{Nu_{serpentine}}{Nu_{straight}} \tag{12}$$

where $Nu_{serpentine}$ and $Nu_{straight}$ are the Nusselt numbers (based on hydraulic mean diameter) for the serpentine channel and for a straight pipe of the same path length, respectively. Note that e_{Nu} can be evaluated locally, at a given axial location or as a mean value using h, $\bar{h}_s$ and $\bar{h}_M$, respectively.

The value of $Nu_{straight}$ depends on the wall thermal boundary condition. For the H2 boundary condition, we use $Nu_{H2} = 2.923$ [5]. The methodology described above was used to simulate fully-developed flow in a straight channel with semi-circular cross-section in order to obtain the fully-developed friction factor and Nusselt number for both the H2 and T boundary condition. We obtain $Nu_{H2} = 2.921(\pm 0.001)$ which is close to the value quoted in Shah and London [5], and $Nu_T = 3.323(\pm 0.001)$, which is close to the value of Ben-Ali et al. [9] and Trupp and Lau [10]. Typical sources of error in CFD simulations include precision error, discretisation error (numerical diffusion and dispersion), and poorly converged solutions. In the determination of the fully developed Nusselt number and friction factor, we minimise round-off error by using double-precision in our calculations. Discretisation error was limited through the use of a second (even-) order bounded differencing scheme with a fine structured mesh. Excellent convergence was achieved for all runs, with normalised residuals being much lower than 10^{-6}. This, together with the high accuracy with which we could reproduce analytic solutions for straight pipe sections, gives us a high degree of confidence in the accuracy of the solution. This resolves the significant uncertainty existing in the value of the Nusselt number for the T boundary condition [6].

The relative pressure-drop penalty incurred for a serpentine passage relative to a straight passage is given by

$$e_f = \frac{(\bar{p}_{in} - \bar{p}_{out})_{serpentine}}{(\bar{p}_{in} - \bar{p}_{out})_{straight}} = \frac{f_{serpentine}}{f_{straight}} \quad (13)$$

where $\bar{p}_{in}$ and $\bar{p}_{out}$ are the area-averaged outlet and inlet pressures, respectively, with

$$\bar{p} = \frac{1}{A_s}\int_{A_s} p_{x,y}\,dA \quad (14)$$

Through simulation, we obtain a straight pipe friction factor of $fRe = 15.771(\pm 0.001)$ which is in good agreement with the value found in [6].

4. Effect of Reynolds number

Heat transfer enhancement and relative pressure-drop penalty are reported for a range of Reynolds numbers up to 450, with $L/d = 4.5$ and $R_c/d = 1$. Reynolds numbers above 450 produced unsteady flow. The effect of Reynolds number on heat transfer enhancement and relative pressure-drop penalty is shown in Fig. 4 for both the H2 and T thermal boundary conditions, with water ($Pr = 6.13$) as the working fluid.

Across the range studied, a very similar dependence on Reynolds number is found for both the T and H2 thermal boundary conditions. At low Reynolds numbers, the thermo-hydraulic characteristics of the serpentine channel approach those of a straight channel of the same length ($e \to 1$). With increasing Reynolds number, the heat transfer coefficient and friction factor increase relative to their values in straight sections, with the enhancement of the heat transfer rate exceeding the relative pressure-drop penalty by a factor of about 2.5 just prior to the onset of unsteady flow.

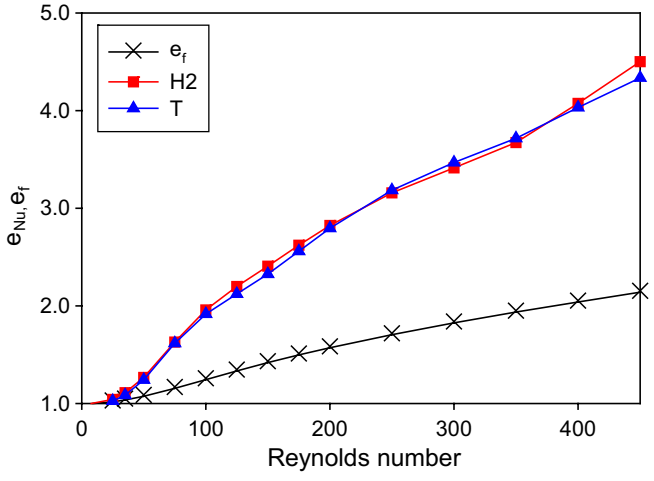

Fig. 4. Mean heat transfer enhancement and relative pressure-drop penalty as a function of Reynolds number for $L/d = 4.5$, $R_c/d = 1$ and $Pr = 6.13$.

4.1. Discussion

As seen in Fig. 5, convective enhancement increases with Prandtl number. Kalb and Seader [1] have shown that the Nusselt number is proportional to Pr^n, with $n \sim 0.2$ in the range $0.7 < Pr < 175$ for curved ducts of circular cross-section. The present results for the serpentine channel with semi-circular cross-section indicate a Prandtl number dependence of $n \sim 0.3$ for $Re > 100$. This dependence is shown in Fig. 6 for $Re = 200$.

Kalb and Seader [1] and Masliyah and Nandakumar [2] both describe an "efficiency" or "enhancement" factor as the ratio of heat transfer enhancement to the relative pressure-drop penalty. As with these authors, we find factors larger than unity for Prandtl numbers greater than 0.7. For low Prandtl number (0.7), relative pressure-drop

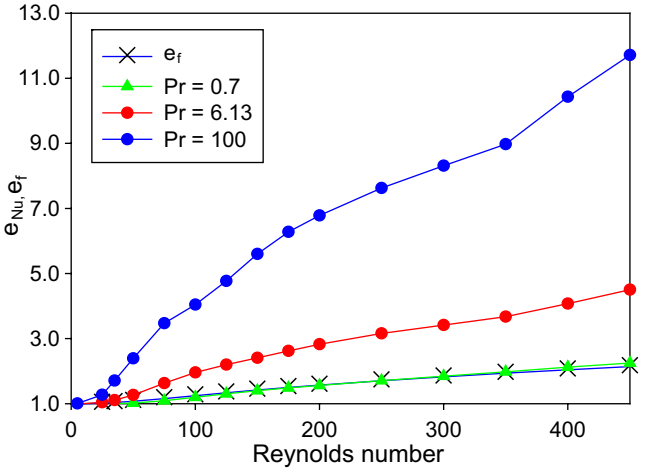

Fig. 5. Mean heat transfer enhancement and relative pressure-drop penalty as a function of Prandtl number for $L/d = 4.5$, $R_c/d = 1$ for the H2 boundary condition.

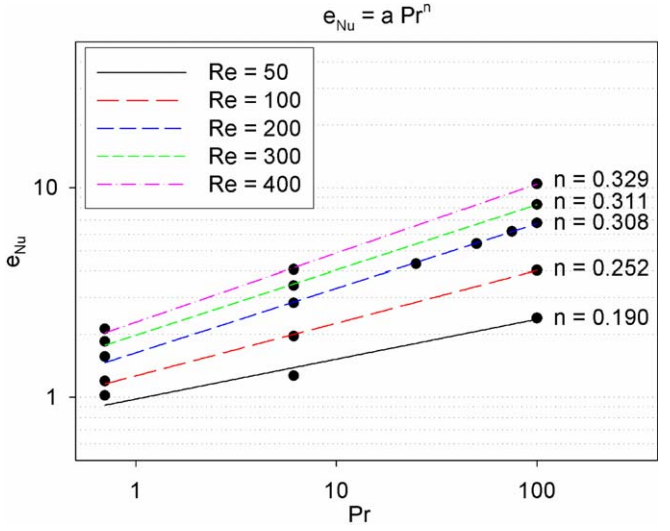

Fig. 6. The effect of Prandtl number on heat transfer enhancement for $Re = 200$, $L/d = 4.5$ and $R_c/d = 1$.

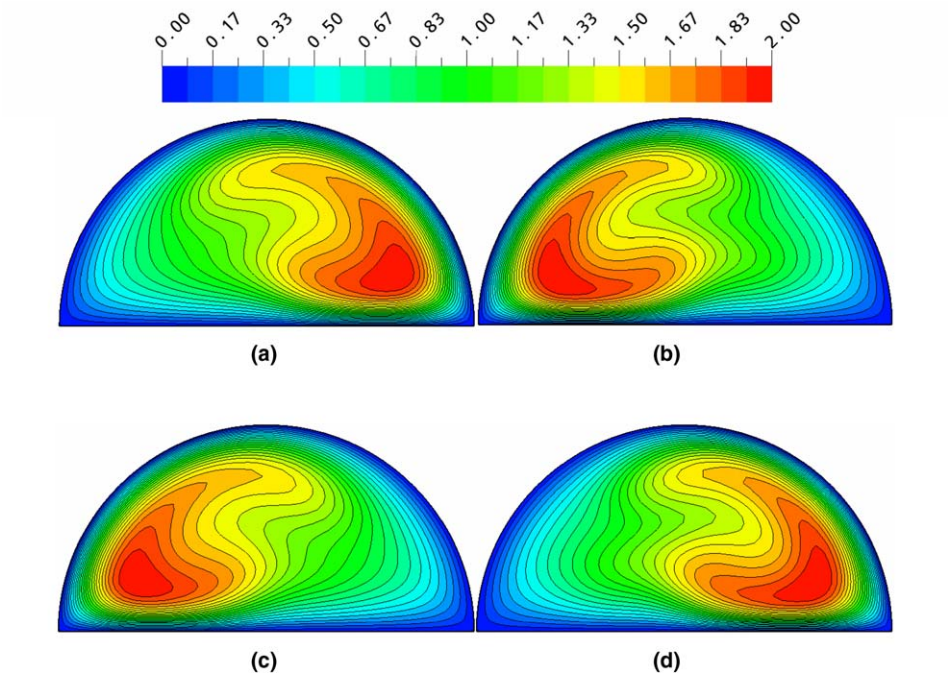

Fig. 7. Speed contours (v/v_M) at various downstream locations for $Re = 200$, $L/d = 4.5$ and $R_c/d = 1$ at: (a) 1d downstream of Bend 1, (b) 1d downstream of Bend 2, (c) 1d downstream of Bend 3, (d) 1d downstream of Bend 4.

penalty and heat transfer enhancement are almost identical in shape and magnitude (Fig. 7).

4.1.1. Flow behaviour

Flow within the serpentine channel displays a number of interesting characteristics which explain the heat transfer results presented above. A transfer of momentum towards the outer wall occurs at a bend, subsequently producing rotation of the fluid about an axis parallel to the bulk flow, resulting in the formation of vortices. These rotating flow features, first observed by Dean [11], and subsequently named Dean vortices, alternate in their direction of rotation following every second bend. Bends 2 and 3 in Fig. 1 are in the same sense. For this reason, Bends 1 and 3 will be referred to as curvature-reinforcing bends, whilst Bends 2 and 4 are known as alternating or cancelling bends. Alternating bends disrupt the secondary flow structures and causes a reversal in rotation direction. The effect of secondary flows on the velocity field at various downstream locations is shown in Fig. 7. The transfer of momentum causes a shift in the maximum fluid speed to the outside of each bend, with the shape of the speed contours being a direct result of the secondary flow structures within the geometry. A reversal in vortex rotation direction following alternating or cancelling bends is evident from Fig. 7(a)–(d). The reversal of vortex direction has been suggested by Schönfeld and Hardt [3] as a possible means to stir and mix a fluid efficiently.

Previous studies [1,4] have shown that secondary flow within channels can retard the onset of flow separation, unsteady flow and turbulence. Here, small regions of reverse flow are evident only at Reynolds numbers beyond 350. These regions occur on the inner radius of cancelling bends, and have a length of less than one diameter in the flow direction.

The characterisation of Dean vortices by a Dean number, expressed as

$$Dn = Re\left(\frac{d}{R_c}\right)^{1/2} \tag{15}$$

shows that for a fixed ratio of duct size (d) to radius of curvature (R_c), the Dean number is directly proportional to the Reynolds number. The Dean number gives a measure of the importance of inertial and centrifugal forces relative to viscous forces. Fig. 8 shows the effect of Reynolds number and secondary flow on the velocity field within the serpentine channel. At low Reynolds numbers (hence low Dean numbers), (Fig. 8(a)), the flow tends towards the straight pipe solution. There is negligible secondary flow as the viscous forces are large in comparison with inertial forces, and act to suppress secondary flow formation. This is consistent with the lack of enhancement of heat transfer or pressure drop at low Reynolds number, as seen in Figs. 4 and 5. As the Reynolds number increases and inertial forces become significant and a single vortex develops. Flow complexity, as well as the number and strength of vortices, increases with Reynolds number. This can be seen in Figs. 8(b)–(f) and 9.

The flow produces a single pair of vortices at Reynolds numbers as low as 50. These decay rapidly along the straight sections within the geometry. As the Reynolds number is increased further, complex secondary flow

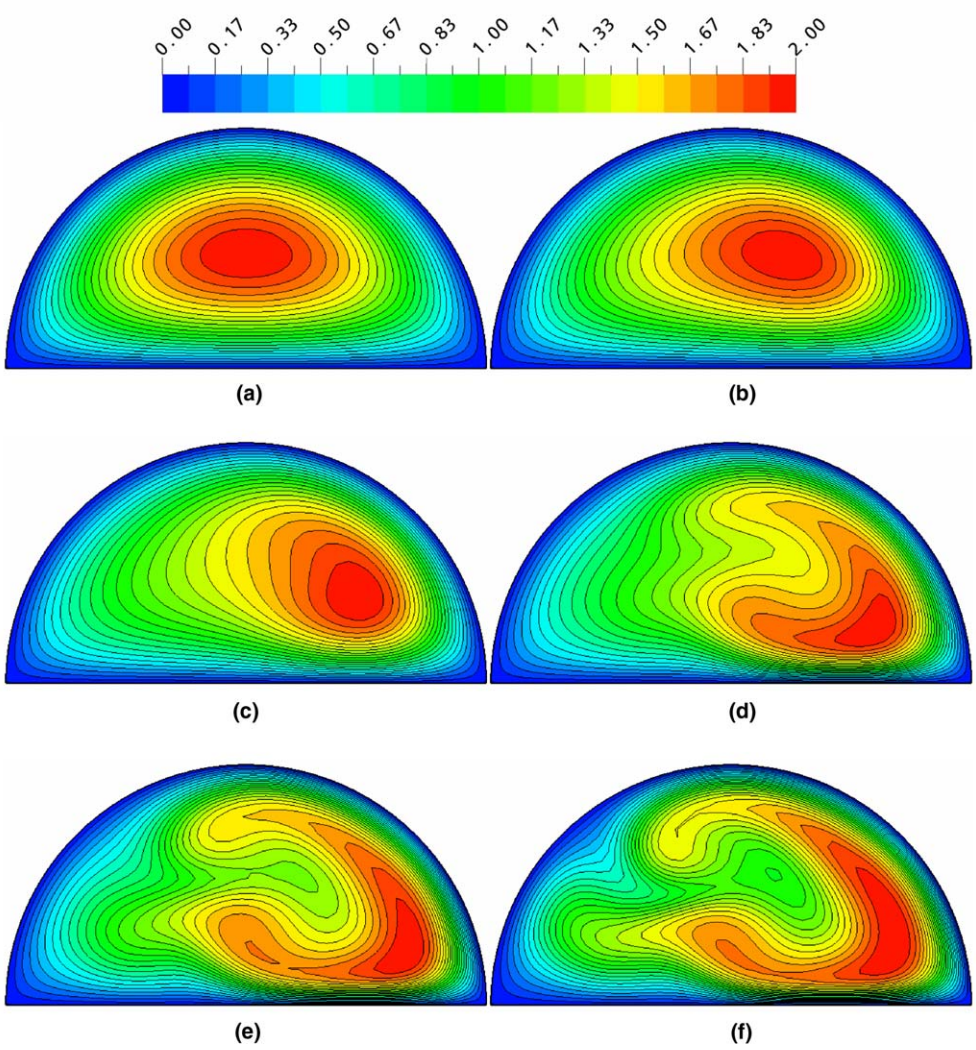

Fig. 8. Speed contours (v/v_M) at the inlet for $L/d = 4.5$, $R_c/d = 1$ and Reynolds numbers of: (a) 5, (b) 50, (c) 100, (d) 200, (e) 300 and (f) 400.

patterns are created, with up to five unclosed vortices being present. This can be seen in the streak-lines in Fig. 9. Secondary flow patterns provide the means to increase the rate of mixing, as seen from the temperature field of Fig. 9. This figure shows hot fluid being transported away from the walls into the centre of the cross-section, with secondary flows disrupting the thermal boundary layer. Local hot spots occur in regions of slow flow, decreasing the rate of local heat transfer for this H2 boundary condition.

4.1.2. Helicity

Levy et al. [12] define a "normalised helicity" to detect and visualise vortex cores as

$$H_n = \frac{\mathbf{v}\cdot\boldsymbol{\omega}}{|\mathbf{v}||\boldsymbol{\omega}|} \tag{16}$$

This quantity has limiting values of ± 1 when the angle between the velocity and vorticity vectors is zero, its sign depending on the direction of rotation about the flow direction. A high value corresponds to a stronger overall alignment between vorticity and velocity vectors and indicates more pervasive vortical structures.

The volume-average of the absolute value of helicity, given by

$$\overline{H}_V = \frac{1}{V}\int_V |H_n| dV = \frac{1}{V}\int_V \frac{|\mathbf{v}\cdot\boldsymbol{\omega}|}{|\mathbf{v}||\boldsymbol{\omega}|} dV \tag{17}$$

is shown in Fig. 10. The absolute value of helicity is used to exclude rotation direction information. The figure shows that volume-averaged helicity increases monotonically across the range of Reynolds numbers studied, corresponding to the continual increase in heat transfer enhancement shown in Figs. 4 and 5.

Fig. 11 shows regions where normalised helicity is high for a range of Reynolds numbers. Flow development within straight sections of the geometry causes a decrease in vortex strength. As the Reynolds number increases, the distance that vortices survive into the straight sections of the pipe also increases. Vortex strength is also dependent on location within the geometry, and is greatest immediately after Bends 1 and 3. Vortices are able to progress

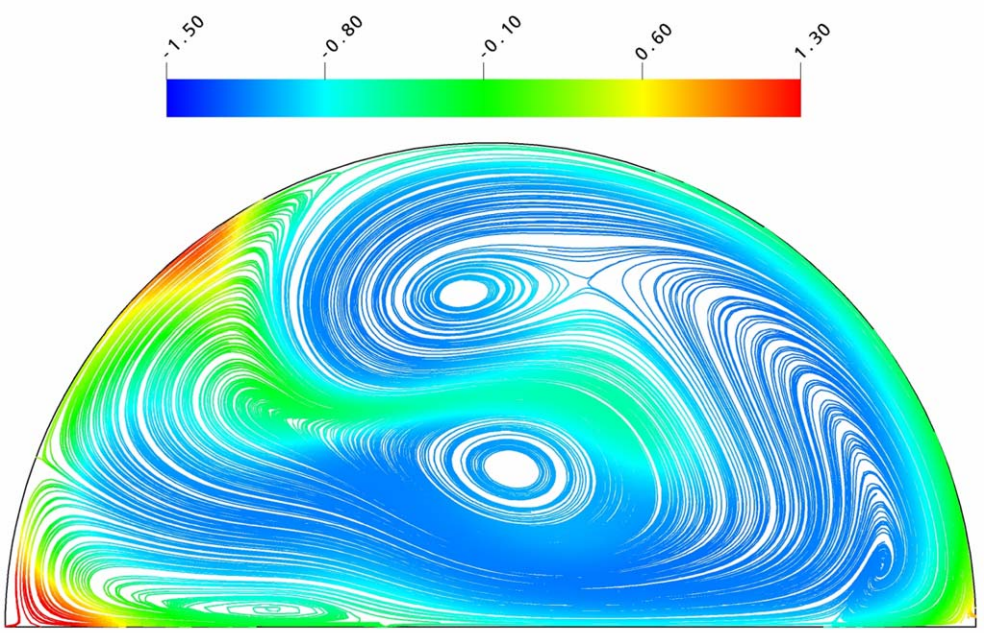

Fig. 9. Streak-lines coloured with non-dimensional temperature (θ) at the inlet for $L/d = 4.5$, $R_c/d = 1$ and a Reynolds number of 400 for the H2 boundary condition.

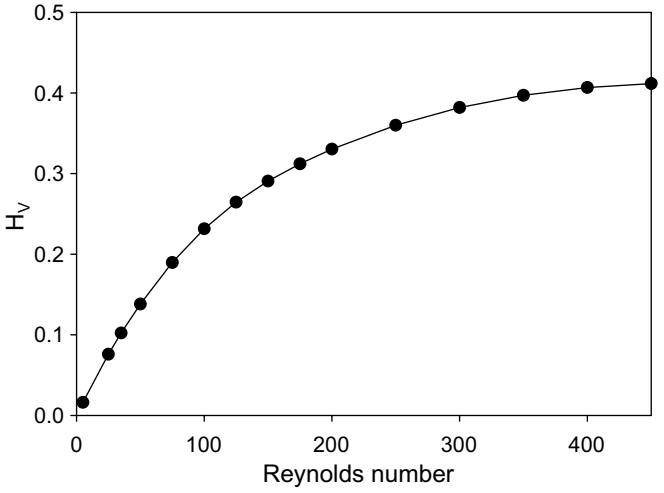

Fig. 10. Effect of Reynolds number on volume integral of the absolute value of normalised helicity for $L/d = 4.5$, $R_c/d = 1$.

through these reinforcing bends with the same direction of rotation, thus acting to increase the vortex strength, which in turn increases the distance they progress into the straight sections of the pipe.

4.1.3. Local heat transfer behaviour

Non-dimensional temperature profiles (Fig. 12) across the serpentine channel show a maximum value at the wall closest to the outside of each bend for low Prandtl numbers. As the Prandtl number is increased, a larger proportion of the channel circumference is in contact with high temperature fluid, as the non-dimensional temperature becomes more uniform across the section, as seen in Fig. 12(c).

Fig. 13 shows how the perimeter-averaged heat transfer enhancement varies through the serpentine modules for different values of Reynolds number. It can be seen that the effect of bends is to promote heat transfer, followed by flow development in the straight section during which the heat transfer enhancement relaxes towards that for fully developed flow in a straight pipe. At low Reynolds number ($Re < 50$), flow and heat transfer remain close to the straight pipe solution, resulting in enhancement values close to unity. The benefit of reinforcing bends becomes apparent when examining the local heat transfer enhancement shown in Fig. 13. Heat transfer enhancement is much larger in the region of reinforcing bends, as secondary flow structures progress through the bends with the same rotational sense. The presence of flow separation at Reynolds numbers above 350 explains the rapid decrease in heat transfer enhancement immediately after cancelling bends.

Fig. 14 displays the peripheral variation of the local heat transfer coefficient (as e_{Nu}) at one diameter downstream of Bend 1 (reinforcing bend), Bend 2 (cancelling bend) and Bend 3 (reinforcing bend). It is important to note that local wall temperatures are used in calculating the local heat transfer coefficients, resulting in large values of enhancement. This is a result of the H2 boundary condition, and is not evident in peripherally-averaged values of heat transfer coefficients which employ $\overline{T}_w$. As seen in this figure, the heat transfer is most strongly enhanced on the flat surface of the cross-section as cold fluid near the centre of the duct is convected to this surface, acting to disrupt the thermal boundary layer, resulting in large heat transfer coefficients.

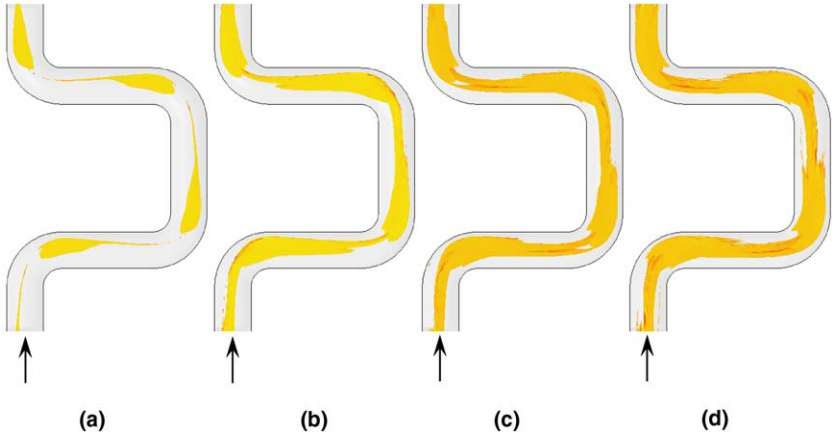

Fig. 11. Isosurface plots of regions where the absolute value of helicity is 0.8 for Reynolds numbers of: (a) 100, (b) 200, (c) 300 and (d) 400. $L/d = 4.5$ and $R_c/d = 1$. The arrows indicate the inlet of the unit. The figure shows the growing region of the duct that is occupied with fluid of high helicity.

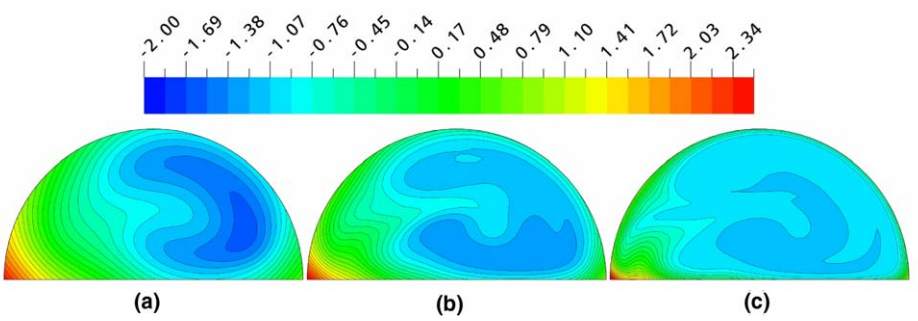

Fig. 12. Non-dimensional temperature contours at inlet for (a) $Pr = 0.7$, (b) $Pr = 6.13$, and (c) $Pr = 100$. $Re = 200$, $L/d = 4.5$ and $R_c/d = 1$ with the H2 thermal boundary condition.

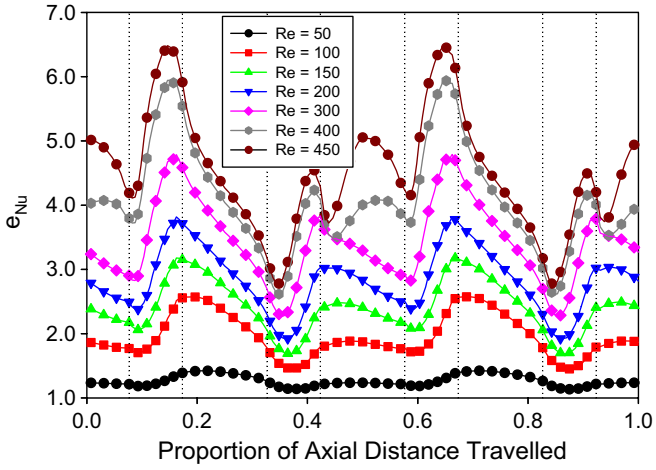

Fig. 13. Heat transfer enhancement as a function of position within a serpentine unit for a Reynolds number of 110, $R_c/d = 1$, $Pr = 6.13$ and $L/d = 4$, 8 and 12.5, for the H2 boundary condition. Dashed lines indicate the relative position of bends.

As vortices are able to progress through reinforcing bends with the same direction of rotation, heat transfer enhancement is larger entering reinforcing bends than alternating bends. This is reflected in Fig. 13. Fig. 14 shows that reinforcing bends enhance heat transfer in a similar fashion, with the shape of the curves being mirror images, symmetric about the middle of the curved surface. The cancelling bend causes enhancement to occur on the opposite side of the channel to the previous bend.

5. Effect of geometric variation

The two independent parameters of L/d and R_c/d have been used to assess the effect of geometric variation on relative pressure-drop penalty and heat transfer enhancement for geometries with a constant unit size ($2L$). The Reynolds number used in this study was 110, chosen as a value for which a single pair of Dean vortices is obtained.

Fig. 15 shows the effect of the ratio of unit size to diameter (L/d) on shape, heat transfer enhancement and relative pressure-drop penalty. The thermal entrance length in straight passages with semi-circular cross-sections, where $e_{Nu} \rightarrow 1.05$, is $L_{th}/d_h \sim 0.1RePr$ [13], or about 67 for the conditions of Fig. 15. For increasing values of L/d at fixed R_c/d, the straight runs between bends become longer. Flow development in these longer straight sections causes relaxation of heat transfer enhancement toward unity, i.e. towards the value for straight pipe flow. The differences shown in local heat transfer enhancement resulting from reinforcing and cancelling bends in Fig. 13 decrease with increasing L/d due to this flow development.

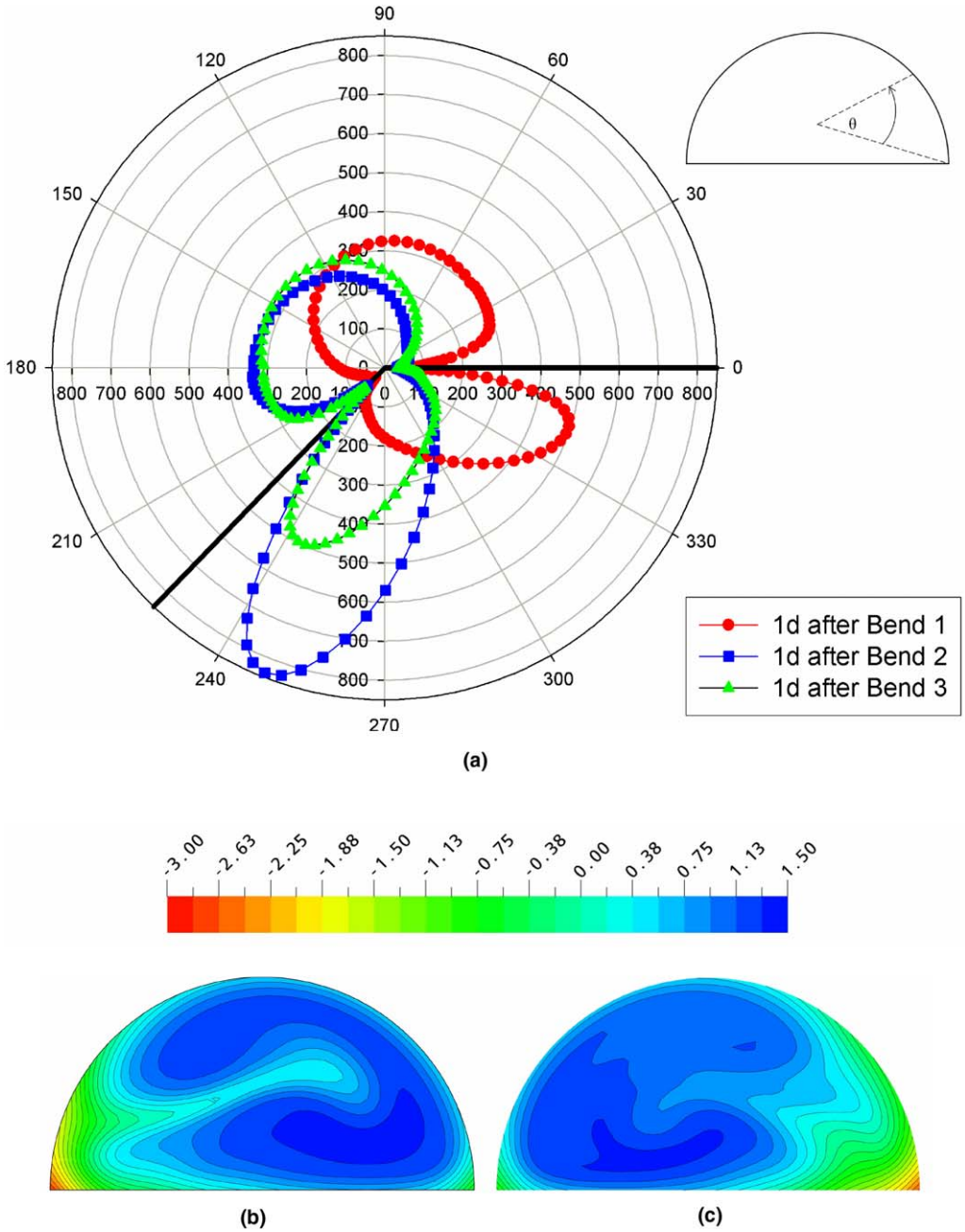

Fig. 14. (a) Relative magnitude of local heat transfer enhancement as a function of peripheral location at a cross-section 1d downstream of Bends 1–3 for a Reynolds number of 200, $L/d = 4.5$, $R_c/d = 1$, $Pr = 6.13$, for the H2 boundary condition. Bold lines indicate corners within the cross-section, and the point of reference is given. Non-dimensional temperature profiles shown at 1d downstream of (b) Bend 1 and (c) Bend 2.

The effects of radius of curvature are displayed in Fig. 16. The minimum physical value for R_c/d is 0.5, which corresponds to a sharp corner on the inside of each bend, however, the lowest value studied here was 0.525 because the sharp corners could not be generated using a swept mesh. A decrease in R_c/d leads to greater heat transfer enhancement and a concomitant rise in relative pressure-drop penalty, as shown in Fig. 16.

As the value of R_c/d decreases, bends become sharper and the straight sections between bends grow longer. Smaller radii of curvature result in pronounced increases in heat transfer enhancement immediately downstream of bends. These are offset by flow development in the longer straight sections.

Low values of R_c/d result in increased pressure losses due to the formation of Dean vortices and flow separation [14]. For the conditions of Fig. 16, flow separation is evident near to the inside curve of each bend when R_c/d is less than 0.8, which coincides with the R_c/d value at which flow separation occurs for serpentine passages with circular

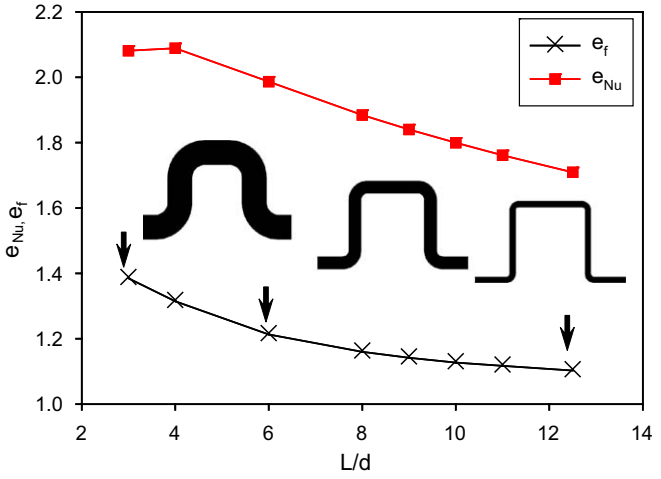

Fig. 15. Mean heat transfer enhancement and relative pressure-drop penalty as a function of L/d. $Re = 110$, $R_c/d = 1$ and $Pr = 6.13$ for the H2 boundary condition.

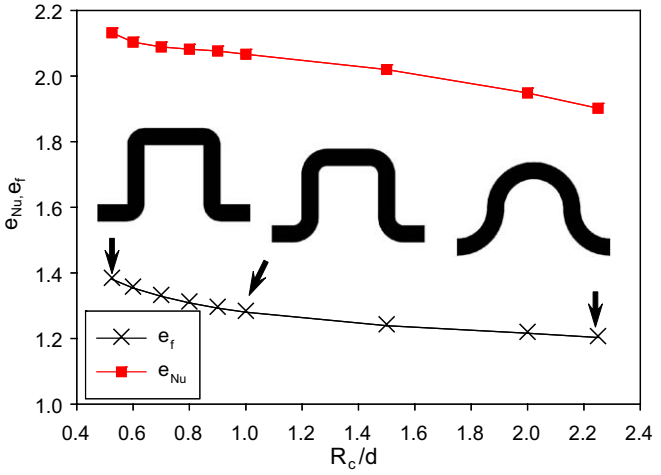

Fig. 16. Mean heat transfer enhancement and relative pressure-drop penalty as a function of R_c/d. $L/d = 4.5$, $Re = 110$, $= 1$ and $Pr = 6.13$ for the H2 boundary condition.

cross-sections [4]. These separated regions are more pronounced following cancelling bends, but their relative length is less than one diameter in the flow direction. Larger increases in relative pressure-drop penalty at values of R_c/d less than 0.8 can be attributed to this flow separation.

The present results for serpentine channels with semi-circular cross-sections may be compared with those for circular cross-sections [4]. Similarities include similar magnitudes of mean heat transfer enhancement, the onset of flow separation occurring at the same value of R_c/d and geometric variation revealing similar effects on heat transfer enhancement and pressure-drop penalties. The serpentine channel with semi-circular cross-section, however, generates greater flow complexity, a delay in the onset of unsteady flow, as well as a less distinct difference in mean heat transfer enhancement for the T and H2 boundary conditions.

6. Conclusions

The methodology developed in earlier work by Rosaguti et al. [4] has been used to study fully-developed laminar flow behaviour in serpentine channels of semi-circular cross-section for both constant wall heat flux (H2) and constant wall temperature (T). The formation of Dean vortices and the inhibition of flow separation in these sections leads to significant heat transfer enhancement without incurring great pressure-drop penalty. The ratio of heat transfer coefficient to friction factor is up to 5.5 times greater than the corresponding ratio in straight passages.

Results have been presented for a range of Reynolds number (5–450), Prandtl number (0.7–100) and geometric configurations ($0.525 < R_c/d < 2.25$, $3 < L/d < 12.5$). Reynolds numbers above 450 produce unsteady flow. For $L/d = 4.5$, $R_c/d = 1$, the rate of heat transfer relative to fully-developed flow in a straight pipe increases with Reynolds number. Enhancement of convective heat transfer is more pronounced at higher Prandtl numbers, with enhancement factors varying approximately as $Pr^{0.3}$ and exceeding a factor of 10 at $Pr = 100$.

Geometric influences on the thermo-hydraulic performance of these channels have been assessed by varying the independent geometric parameters of L/d and R_c/d for a fixed Reynolds number. Increasing L/d decreases both heat transfer enhancement and relative pressure-drop penalty, with performance approaching that of a straight pipe at high L/d. Heat transfer enhancement and relative pressure-drop penalty also decrease with an increase in R_c/d.

Acknowledgement

The authors acknowledge the support of Heatric, the Australian Research Council for an APAI scholarship for Nathan Rosaguti, and Patrick Sharkey of ANSYS CFX for assistance with the wrapping code. This work is supported by Heatric/Meggitt PLC.

References

[1] C.E. Kalb, J.D. Seader, Heat and mass transfer phenomena for viscous flow in curved circular tubes, Int. J. Heat Mass Transfer 15 (4) (1972) 801–817.
[2] J.H. Masliyah, K. Nandakumar, Fully developed viscous flow and heat transfer in curved semi-circular sectors, AIChE J. 25 (3) (1979) 478–487.
[3] F. Schönfeld, S. Hardt, Simulation of helical flow in microchannels, AIChE J. 50 (4) (2004) 771–778.
[4] N.R. Rosaguti, D.F. Fletcher, B.S. Haynes, Laminar flow and heat transfer in a periodic serpentine channel, Chem. Eng. Technol. 28 (3) (2005) 353–361.
[5] R.K. Shah, A.L. London, in: T.F. Irvine, J.P. Hartnett (Eds.), Advances in Heat Transfer, Supplement 1, Laminar Flow Forced Convection in Ducts, Academic Press, New York, 1978.
[6] R.M. Manglik, A.E. Bergles, Fully developed laminar heat transfer in circular-segment ducts with uniform wall temperature, Numer. Heat Transfer, Part A (26) (1994) 499–516.

[7] E.M. Sparrow, A. Haji-Sheikh, Laminar heat transfer and pressure drop in isosceles triangular, right triangular and circular sector ducts, ASME J. Heat Transfer 87 (1965) 426–427.
[8] ANSYS, CFX Computational Fluid Dynamics (CFD) software, 2005. Available from: <www.ansys.com/cfx>.
[9] T.M. Ben-Ali, H.M. Soliman, E.K. Zariffeh, Further results for laminar heat transfer in annular sector and circular sector ducts, ASME J. Heat Transfer 111 (1989) 1090–1093.
[10] A.C. Trupp, A.C.Y. Lau, Fully developed laminar heat transfer in circular sector ducts with isothermal walls, ASME J. Heat Transfer 106 (1984) 467–469.
[11] W.R. Dean, Note on the motion of fluid in a curved pipe, The London, Edinburgh and Dublin Philosophical Magazine 7 (14) (1927) 208–223.
[12] Y. Levy, D. Degani, A. Seginer, Graphical visualization of vortical flows by means of helicity, AIAA J. 28 (8) (1990) 1347–1352.
[13] Q.M. Lei, A.C. Trupp, Forced convection of thermally developing laminar flow in circular sector ducts, Int. J. Heat Mass Transfer 33 (8) (1990) 1675–1683.
[14] D.F. Young, B.R. Munson, T.H. Okiishi, A Brief Introduction to Fluid Mechanics, third ed., John Wiley & Sons, Inc., NJ, 2004.